

Article

# Temperature Modulation of MOS Sensors for Enhanced Detection of Volatile Organic Compounds

Andrea Rescalli <sup>1,†</sup>, Davide Marzorati <sup>2,†</sup>, Simone Gelosa <sup>3</sup>, Francesco Cellesi <sup>3</sup> and Pietro Cerveri <sup>1,4,\*</sup>

<sup>1</sup> Department of Electronics, Information, and Bioengineering, Politecnico di Milano, 20133 Milan, Italy; andrea.rescalli@polimi.it

<sup>2</sup> Department of Technology and Innovation, Institute of Digital Technologies for Personalised Healthcare, University of Applied Sciences and Arts of Southern Switzerland, 6962 Lugano, Switzerland; davide.marzorati@supsi.ch

<sup>3</sup> Department of Chemistry, Materials and Chemical Engineering “Giulio Natta”, Politecnico di Milano, 20133 Milan, Italy; simone.gelosa@polimi.it (S.G.); francesco.cellesi@polimi.it (F.C.)

<sup>4</sup> Istituto Auxologico Italiano IRCCS, 20145 Milan, Italy

\* Correspondence: pietero.cerveri@polimi.it

† These authors contributed equally to this work.

**Abstract:** Disease diagnosis through biological fluids, particularly exhaled breath analysis, has gained increasing importance. Volatile organic compounds (VOCs) present in exhaled breath offer diagnostic potential as they reflect altered and disease-specific metabolic pathways. While gas chromatography–mass spectrometry (GC–MS) has been traditionally used for VOCs detection, electronic noses have emerged as a promising alternative for disease screening. Metal oxide semiconductor (MOS) sensors play an essential role in these devices due to their simplicity and cost-effectiveness. However, their limited specificity and sensitivity pose challenges for accurate diagnosis at lower VOCs concentrations, typical of exhaled breath. To address specificity and sensitivity issues, temperature modulation (TM) has been proposed in this paper, introducing a custom-developed electronic nose based on multiple and heterogeneous gas sensors located within an analysis chamber. Four different TM patterns (i.e., square, sine, triangular, and a combination of square and triangular) were applied to the gas sensors to test their response to three different analytes at three distinct concentrations. Data were analyzed by extracting meaningful features from the sensor raw data, and dimensionality reduction using principal component analysis (PCA) was performed. The results demonstrated distinct clusters for each experimental condition, indicating successful discrimination of analytes and concentrations. In addition, an analysis of which set of sensors and modulation pattern yielded the best results was performed. In particular, the most promising TM pattern proved to be the square and triangular combination, with optimal discrimination accuracy between both concentrations and analytes. One specific sensor, namely, TGS2600 from Figaro USA, Inc., provided the best performance. While preliminary results highlighted the potential of TM to improve the sensitivity of gas sensors in electronic nose devices, paving the way for further advancements in the field of exhaled breath analysis.

**Keywords:** exhaled breath analysis; electronic nose; temperature modulation; metal oxide sensors



**Citation:** Rescalli, A.; Marzorati, D.; Gelosa, S.; Cellesi, F.; Cerveri, P. Temperature Modulation of MOS Sensors for Enhanced Detection of Volatile Organic Compounds. *Chemosensors* **2023**, *11*, 501. <https://doi.org/10.3390/chemosensors11090501>

Academic Editor: Pi-Guey Su

Received: 2 August 2023

Revised: 8 September 2023

Accepted: 13 September 2023

Published: 15 September 2023



**Copyright:** © 2023 by the authors. Licensee MDPI, Basel, Switzerland. This article is an open access article distributed under the terms and conditions of the Creative Commons Attribution (CC BY) license (<https://creativecommons.org/licenses/by/4.0/>).

## 1. Introduction

Since the last decade, the significance of disease diagnosis through the analysis of biological fluids has been rapidly increasing [1–3]. Notably, conditions such as lung cancer, chronic obstructive pulmonary disease, prostate cancer, and asthma are among the various diseases that can be diagnosed through this approach [4–9]. The most common biological fluid that is analyzed to achieve disease diagnosis is exhaled breath. It consists of a liquid phase, composed of aerosol particles made of non-volatile organic compounds, and a gaseous phase, containing volatile organic compounds (VOCs) [10]. The latter are

produced at the cellular level, released into the bloodstream, and eventually expelled from the body through exhalation [11]. Diseases, altering cellular metabolic pathways, induce modifications of the amount and type of volatile compounds [12,13]. Hence, such unique changes in VOCs profiles offer valuable insights for disease detection through exhaled breath. Their concentration could also be related to disorder staging [14]. Various alcohols, ketones, and hydrocarbons have been detected in exhaled breath and correlated to different clinical conditions [2]. However, the challenge in using exhaled breath as a diagnostic tool is that the concentration of disease-related volatile compounds is very low, typically in the parts per billion (ppb) range [15,16]. Early scientific studies on exhaled breath analysis for disease diagnosis predominantly relied on classical GC–MS methods for compound detection [17–21]. While GC–MS methods offer compound-specific detection at very low concentrations, they are not suitable for screening purposes. Hence, in the latest years, researchers have started exploring technological alternatives to GC–MS for exhaled breath analysis [2,22,23]. Electronic noses are an example of devices being investigated as a screening tool for disease diagnosis, even at early stages [24]. Unlike conventional and expensive GC–MS equipment, electronic noses do not provide absolute concentration values for each compound in the sample but rather generate a signal representing the combined response of all VOCs in the mixture under analysis. On the market, there exist commercially available devices acting as electronic noses, such as the Cyranose 320 and the Aeonose electronic noses, both proposed for gas analysis [25]. Various sensing technologies, such as quartz microbalances [26,27], gold nanoparticles [28], MOS [25], and colorimetric sensors [29,30], can be employed in the design and development of sensors for electronic noses. Sensors can be designed to target a specific compound, leading to VOCs-specific analysis. However, it is still unclear in clinics whether a single compound or a mixture of compounds is functional to disease diagnosis [20,21]. Among different sensing approaches, MOS sensors have been largely used in electronic noses. These sensors consist of a tin dioxide layer placed over a substrate, kept at a certain working temperature through a heater component [31]. The variable that is measured through such sensors is their resistance, which decreases or increases depending on whether the sensor is configured as an n-type or p-type MOS, respectively. An example of a MOS sensor response is reported (Figure 1). High power is required to operate these sensors, as the working temperature ranges between 300 °C and 500 °C [32]. At low temperatures (below 100 °C), in fact, the rate of oxygen reactions occurring on the sensor surface is too low and does not allow for a proper change in the sensor resistance. Despite numerous studies reporting the use of MOS sensors for biological fluid analysis [9,23,33–35], both their limited specificity and low sensitivity are significant drawbacks. Even if these sensors can be tailored to detect specific substances, they also exhibit significant responses to substances they were not designed for. Moreover, many of the commercial sensors that have been used in disease diagnosis show sensitivity values in the parts per million (ppm) range, whereas biomarkers in exhaled breath are typically present at lower concentrations, in the ppb range [21,36,37]. To improve the specificity and the sensitivity of MOS gas sensors, TM of the heating component has been proposed [22,38–42]. The underlying principle is that the change in heater temperature of the sensor can alter the chemical or physical interactions between the analyte and the sensing material, leading to a more pronounced response [42,43]. This increased sensitivity allows the sensor to detect lower concentrations of the target substance [44]. It has also been shown that selectivity enhancement may be gained to reduce overlapping responses of different analytes [42]. However, the existing literature primarily focuses on the use of a few gas sensors and measurements with a single compound. To date, no studies have investigated the feasibility of using TM approaches with mixtures of compounds at different concentrations, which better reflect the composition of biological fluids. In addition, no consensus exists on the optimal TM patterns to be applied to the sensors [42]. In the present manuscript, we described a system able to analyze samples of air through multiple and heterogeneous gas MOS sensors, enabling temperature-modulated patterns through custom electronics. This setup aimed to evaluate the feasibility of improving

the specificity of MOS sensors in detecting different compounds, namely carbon dioxide, methane, and butanone, analyzed at different concentrations. In particular, we analyzed the performances of eight sensors and four different TM patterns in the discrimination of such compounds and decreasing concentrations. Eventually, we achieved the identification of the optimal combination of TM patterns and gas sensors for compound-specific detection.

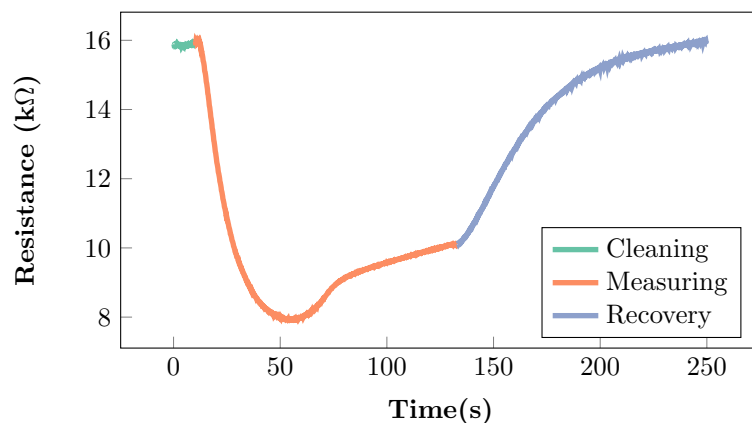


**Figure 1.** Resistance variations of an MOS sensor when exposed to a breath sample, as derived from the literature [2,33,45]. During the *measuring* phase, the sensor is exposed to the breath sample, and the resistance changes with respect to the baseline resistance detected in the *cleaning* phase. The *recovery* phase allows the sensor to return to its baseline.

## 2. Material and Methods

### 2.1. Hardware

The electronic nose consisted of a two-layer custom printed circuit board (PCB), an analysis chamber (with openings for gas inlet and outlet), power control electronics, and two pairs of hydraulic components (air pump and valve), necessary to drive the air undergoing analysis in and out of the chamber (Figure 2a). The sensors were mounted on the bottom layer of the PCB, which hermetically sealed the gas analysis chamber (Figure 2b).

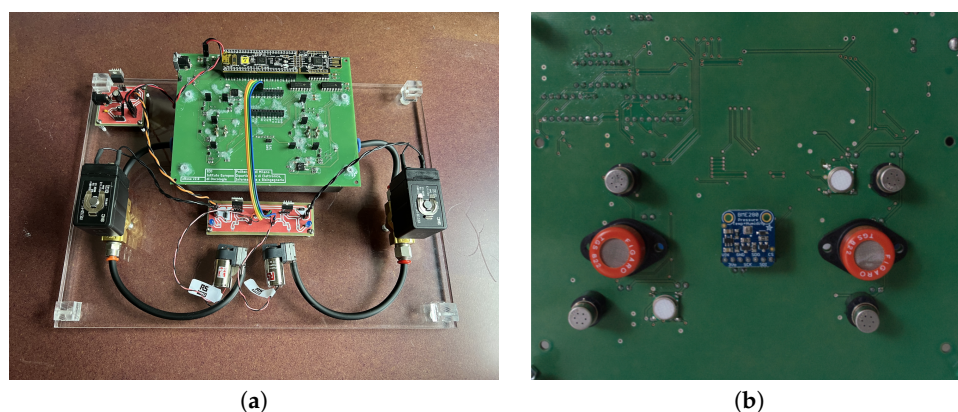


**Figure 2.** (a) Top view of the PCB integrating the circuit for TM of gas sensors, together with the associated components required for its functioning. (b) Bottom view of the temperature-modulated electronic nose, showing the gas sensors and the environmental sensor, located at the center of the board in contact with the analysis chamber.

#### 2.1.1. Gas Sensors

The electronic nose contained eight gas sensors, which could be simultaneously used and temperature modulated independently of each other. Out of the eight sensors, six belonged to the TGS family (Figaro USA, Inc., Rolling Meadows, IL, USA), while the other two were AS-MLV-P2 sensors (Scioscience, Eindhoven, The Netherlands). Sensors S-1,

S-2, S-3, and S-4 were TGS2600 type. Sensors S-5, and S-6 were TGS822 type. Finally, sensors S-7, and S-8 were AS-MLV-P2 type (Table 1). The TGS sensors were mounted on the PCB through sockets (models SR4 and SR6, Figaro USA, Inc.), allowing for easy testing and replacement, while the AS-MLV-P2 sensors were directly soldered onto the board. The TGS sensors were mainly sensitive to organic solvent compounds, such as alcohols (e.g., methanol and propanol) and hydrocarbons (e.g., methane and propane), while the AS-MLV-P2 sensors were sensitive to reducing gases, including carbon oxide, showing selectivity also for hydrocarbons.

**Table 1.** Description of the gas sensors employed in the prototype electronic nose as provided by the respective manufacturer’s datasheets.

Sensor	Sensitivity [ppm]	Target Compounds
TGS2600	1–100	methane, ethanol, hydrogen
TGS822	50–5000	Organic solvent vapors (methane, benzene, ...)
AS-MLV-P2	10–5000	Reducing gases (carbon oxide, methane, ...)

### 2.1.2. Electronics

The main core of the developed electronic nose was the CY8C5888LTI-LP097 microcontroller unit (MCU), part of the PSoC 5LP family, mounted on a kit board, the CY8CKIT-059 (Infineon Technologies, Neubiberg, Germany) [46]. The MCU firmware was in charge of handling all the tasks required for the electronic nose, ranging from the control of the TM up to the acquisition of the sensor responses and their streaming to a host machine. The sensing components mounted on the PCB were not limited to gas sensors. A sensor designed to monitor the environmental air, the BME280 (Robert Bosch GmbH, Gerlingen, Germany) was mounted on the PCB so that temperature, relative humidity, and atmospheric pressure data could be collected [47]. The BME280 sensor also offers the possibility of detecting generic VOCs, but this feature was not exploited in the present work.

The custom PCB integrated an electronic circuit dedicated to the control of the voltage applied to the heater pins of each sensor (Figure 3). Through this circuit, it was possible to apply a TM pattern to each gas sensor.

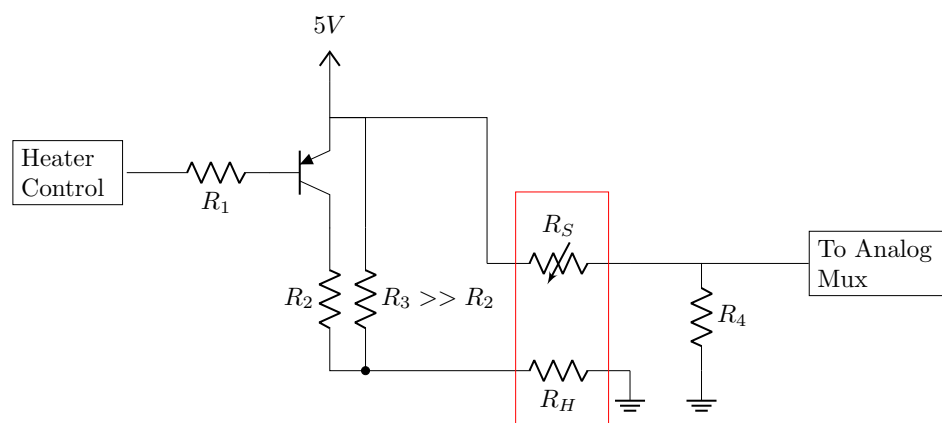


**Figure 3.** Circuit for gas sensor resistance measurement with temperature control. The components embedded in the red rectangle represent the gas sensors, with the variable sensor resistance,  $R_S$ , and the heater resistance,  $R_H$ . The output pin of the microcontroller for heater control and the input pin of the analog mux are also shown.

Four main TM patterns were implemented in the electronic nose firmware, namely square, sinusoidal, triangular, and a combination of square plus triangular patterns (Figure 4). The square pattern (also referred to as *Rect*) had a period of 60 s, with a 50% duty cycle. The sine pattern had a period of 50 s. The triangular pattern had a period of 100 s. The square plus triangular pattern (abbreviated to *ReTr*) had a period of 100 s, with each

sub-pattern lasting 50 s. All patterns had an amplitude ranging from 0 to 5 V. According to the implemented electrical configuration, any pattern could be applied directly to the heater control pin of each gas sensor (Figure 3). Notably, despite being called *temperature modulation patterns*, from an electrical point of view they were implemented as voltage control signals. This is due to the nature of the commercial sensors employed, which do not allow for direct control of their working temperature. Temperature can be modulated only through the heater component (the resistor  $R_H$  in Figure 3), and there is no possibility of measuring the real increment or decrement in temperature upon the application of the voltage pattern.

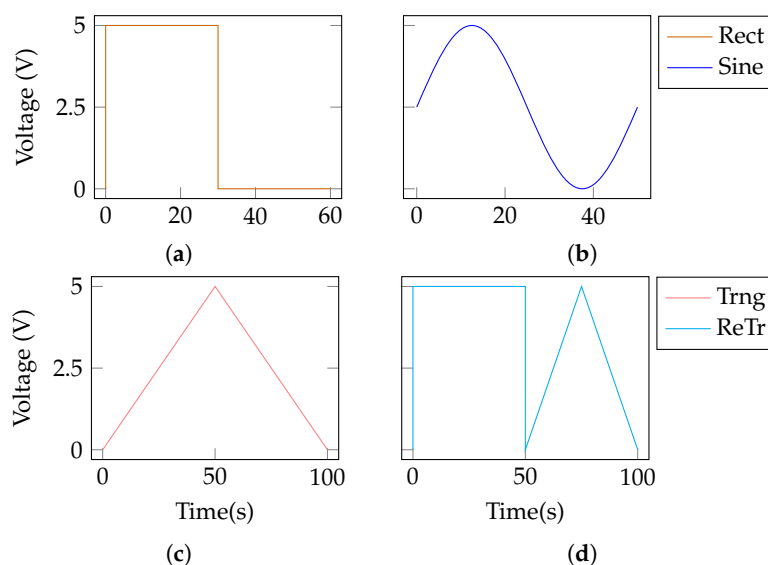


**Figure 4.** Temperature modulation patterns implemented for the control of the heating component of the gas sensors. (a) Rect. (b) Sine. (c) Trng. (d) ReTr.

### 2.1.3. Hydraulic Components

In order to achieve proper movement of the air sample in and out of the analysis chamber, a hydraulic system was implemented. A micro-pump (model D200-03, RS Pro, Corby, UK) and a solenoid valve (VXE Series, SMC Pneumatics, Brugherio, Italy) were placed both at the inlet and at the outlet of the sensor chamber nose (Figure 2a). polytetrafluoroethylene (PTFE) tubes and rapid connectors were used for all the hydraulic connections. The analysis chamber, over which the PCB was positioned, was made of die-cast aluminum with a volume of approximately 500 mL. The experiments were performed in dynamic conditions, with the sample under analysis flowing into the chamber and out of it with an equal flow rate.

### 2.2. Software

In order to control and configure the electronic nose, and also to retrieve the measurement data, custom software was developed, written in Python 3.9 using Kivy 2.1 as the main graphical framework. Communication between the electronic nose and the software running on a host machine was ensured by UART protocol. The software enclosed full control over the settings of the device, such as configurations for the environmental sensor, choice of the TM pattern, valve and pump control, and options for data export and protocol adjustments, as well as the possibility to visualize in real time the sensor data, coming from both the gas and environmental sensors.

### 2.3. Experimental Design

Three chemical compounds were investigated, namely methane ( $\text{CH}_4$ ), carbon dioxide ( $\text{CO}_2$ ), and butanone ( $\text{CH}_3\text{COCH}_2\text{CH}_3$ ). All the analytes were tested in a mixture with nitrogen ( $\text{N}_2$ ) across three different concentrations (75, 130, and 300 ppm). The nitrogen gas

was provided by Sapio company (IT), featuring a purity of 99.9%. The oxygen contaminant level in the nitrogen gas distribution line was measured in the range of about 20 ppm. The target compounds were chosen according to both clinical and technical considerations. Methane and butanone have been documented in the literature as potential biomarkers for gastrointestinal disorders [48,49] and lung cancers [16,50], respectively. Carbon dioxide was chosen because, being a respiration product, it is always present in exhaled breath. On the technical side, sensitivity to methane was explicitly stated by the manufacturers for all the selected sensors (cfr. Table 1), whereas no further information was given for carbon dioxide or butanone. Hence, the performances of these sensors were tested to see whether they could still be used to discriminate between different compounds. In order to achieve the desired concentration values properly and to mix the target compounds, an external hydraulic mixing system was designed, with nitrogen as the carrier gas. A rotameter was calibrated with nitrogen to achieve a constant flow rate of 21 L/min, and a mass flow meter was calibrated with the analyte of interest. Given the nitrogen flow rate,  $F_{N_2}$ , and the flow rate of the target analyte,  $F_T$ , the final concentration of the analyte can be determined using the following equation:

$$C(ppm) = \frac{F_T}{F_{N_2}} \cdot 10^6. \quad (1)$$

Once the target analyte flow was properly set up, all the experiments were carried out with the following steps:

1. *Wash-out* (30 min): the first time a new concentration was about to be tested, the chamber and the sensors were cleaned with a continuous stream of pure nitrogen. During this phase, the gas sensors were heated by applying a constant voltage of 5 V.
2. *Filling* (12 min): each time a wash-out phase was performed, it was followed by a 12-min period in which the target analyte was added to the nitrogen flow and introduced inside the chamber. During this phase, the sensor heaters were kept at 5 V. This step was needed to ensure a uniform concentration of the target inside the chamber before measurements.
3. *Modulation* (70 min approx.): this phase was divided into three parts:
  - *Baseline*: initially, a baseline value for the sensors was measured for 2 min without any pattern applied to the heater.
  - *Measuring*: then, one of the TM patterns was applied for an amount of time sufficient to acquire 10 cycles.
  - *Recovery*: finally, the pattern was interrupted and the heaters were brought back to a constant 5 V for an additional 2 min.

The three steps in the *modulation* phase were repeated for each one of the four modulation patterns before changing the concentration of the target analyte and going back to the *wash-out* phase.

#### 2.4. Data Analysis

Throughout all the experiments that were carried out, data were collected during the *wash-out*, *filling*, and *modulation* phases and saved in CSV format for subsequent analysis. The data related to the measuring sub-phase were composed of gas sensor responses to the analyte of interest, while a given TM pattern was cycled for the overall duration of the sub-phase. Therefore, the first step of the data analysis part was to extract the gas sensor responses to a single TM cycle. An example of a raw sensor response to a single TM cycle is reported (Figure 5).

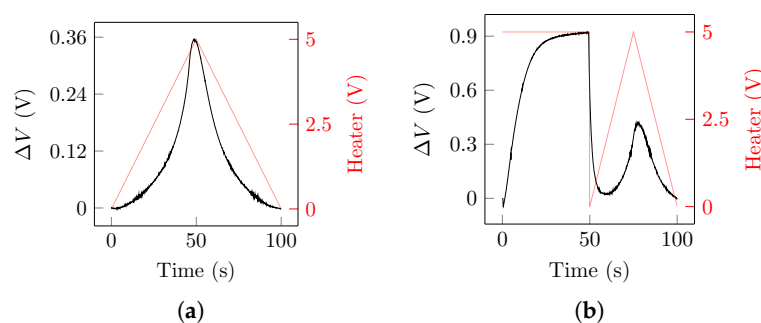


**Figure 5.** (a) Raw sensor data recorded during one cycle of the triangular TM pattern. The data were retrieved from sensor TGS2600 when exposed to butanone with a concentration of 75 ppm. (b) Raw sensor data recorded during one cycle of the ReTr TM pattern. The data were retrieved from sensor TGS2600 when exposed to methane with a concentration of 130 ppm. Black lines show the raw response of the sensor, expressed as the difference ( $\Delta V$ ) between the measured voltage and the voltage measured when the TM was first applied. Red lines show the voltage applied to the heater component.

#### 2.4.1. Feature Extraction

After collecting the voltage data from one single TM cycle, representative features were computed. At first,  $V_{out}$  values were converted to a resistance signal (cfr. Figure 3), according to the following relation:

$$R_S = R_4 \left( \frac{5V}{V_{out}} - 1 \right). \quad (2)$$

From the  $R_S$  resistance signal, hand-crafted features were computed per compound, per concentration of each compound, per sensor, per TM pattern, and per single cycle of TM pattern (Figure 6). The following features were calculated:

- $\Delta_1$ : difference between the maximum resistance value of the sensor during the first half of the TM pattern,  $R_{max}$ , and the baseline resistance value of the sensor at time  $t = 0$ ,  $R_0$ :

$$\Delta_1 = R_{max} - R_0 \quad (3)$$

- $\Delta_2$ : difference between the maximum resistance value of the sensor during the first half of the TM pattern,  $R_{max}$ , and the minimum resistance of the sensor during the second half of the TM pattern,  $R_{min}$ . In the case of the ReTr TM pattern, this feature was computed considering the maximum voltage value during the second half of the TM pattern as  $R_{max}$ :

$$\Delta_2 = R_{max} - R_{min} \quad (4)$$

- **Slope<sub>1</sub>**: ratio between the  $\Delta_1$  value and the time,  $t_1$ , required by the sensor to reach the maximum value. This feature allows describing the dynamics of the sensor and the exposure to the sample:

$$\Theta_1 = \frac{\Delta_1}{t_1} \quad (5)$$

- **Slope<sub>2</sub>**: ratio between the  $\Delta_2$  value and the time,  $t_2$ , required by the sensor to move from the maximum to the minimum value:

$$\Theta_2 = \frac{\Delta_2}{t_2} \quad (6)$$

The computation of the 4 features (i.e.,  $\Delta_1$ ,  $\Delta_2$ ,  $\Theta_1$ , and  $\Theta_2$ ) yielded a data set composed of 2880 observations as they were extracted for each concentration (3), for each compound (3), for each sensor (8), for each TM pattern (4), and for each cycle (10 cycles in total) of the pattern. To facilitate data interpretation, the data set underwent a restructuring process aimed at enhancing its efficiency. As a result, we obtained 10 observations for each concentration of every compound, resulting in a total of 90 observations and 128 features (Figure 6).

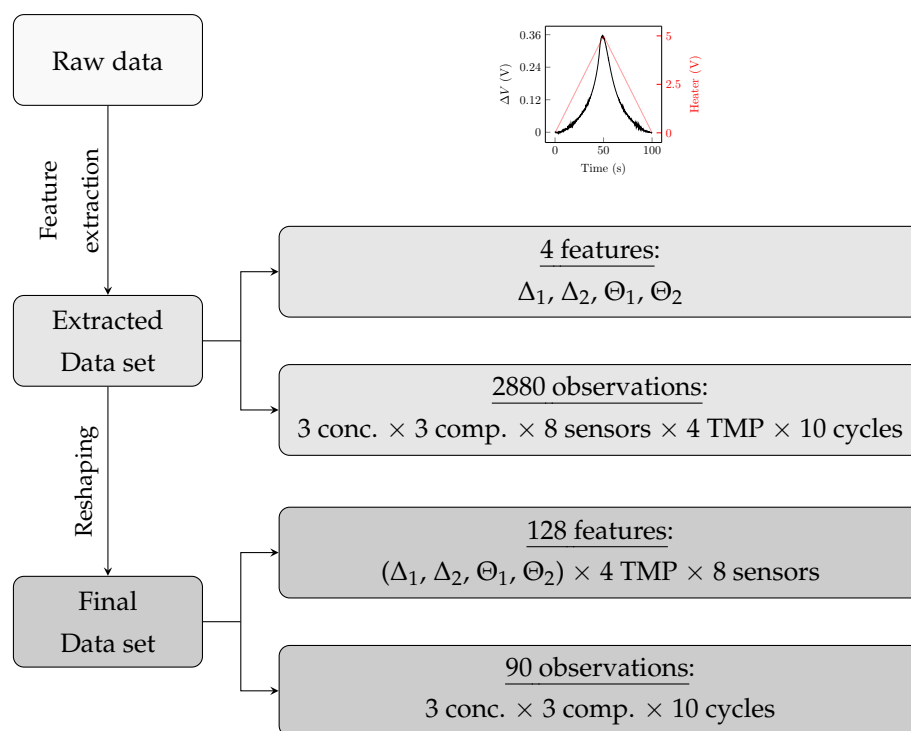


**Figure 6.** Schematic representation of the structure of the data set prior to PCA operation: feature extraction and reshaping processes have been highlighted.

#### 2.4.2. Compound, Concentration, and Sensor Discrimination

After reshaping the features data set into 128 values and 90 observations, principal component analysis (PCA) was applied to reduce the dimensionality of the dataset. Before proceeding with PCA, each feature was normalized using a min–max algorithm. PCA was applied considering each TM pattern independently from the others, and each group of sensors (TGS2600, TGS822, and AS-MLV-P2). In order to evaluate which TM pattern, out of the four, maximized the identification of the three compounds, a 3-cluster k-nearest neighbors (kNN) classifier was applied to the relevant principal components. The data set was split into 80% train and 20% test sets with stratified sampling to maintain proportions between the target classes in the two sets. The classification accuracy was reported to quantify the kNN performance. Likewise, the three groups of sensors were tested using the best TM pattern previously identified by means of the kNN classifier.

### 3. Experimental Results

The experiments were carried out on separate days for each compound, for a total of three days of experiments. The overall time required for the system setup, mostly for the calibration of the rotameter and the mass flow meter, exceeded two hours, and it was compound-specific. All the sensor responses were continuously collected by the electronic nose and sent to the host machine for real-time visualization. Gathered raw data were stored as CSV files for subsequent analysis.

#### 3.1. Features Analysis

The values of the  $\Delta_1$  feature, averaged across the four patterns, were reported for the three analytes, computed from raw data gathered from S-1 (TGS2600), S-6 (TGS822), and S-7 (AS-MLV-P2) sensors across the three concentrations (Table 2). As noticed, the  $\Delta_1$  feature had mostly either increasing or decreasing trends with the increasing concentration, with the scale depending on the specific resistance of the sensor. The distributions of the  $\Theta_2$  feature for the triangle TM pattern in the S-1 (TGS2600) and S-6 (TGS822) sensors were reported (Figure 7). As noticed, butanone induced a decreasing response in the S-1 sensor, from 75 to 300 ppm, whereas methane and carbon dioxide showed an increasing trend with

an increase in concentration.  $\Theta_2$  decreased for all three compounds in the S-6 sensor but with different absolute values. After dimensionality reduction, the cumulative explained variance of the first three principal components, obtained considering all the features derived from the whole set of temperature modulations, and the sensors conveyed more than 80% of the information (Figure 8).

**Table 2.**  $\Delta_1$  feature (arbitrary units) averaged across the four TM patterns as a function of the increasing concentration (ppm).

Sensor	Butanone			CO <sub>2</sub>			CH <sub>4</sub>		
	75	130	300	75	130	300	75	130	300
S-1 (TGS2600)	1400	1103	804.0	288.8	350.8	529.3	376.2	650.7	1021
S-6 (TGS822)	3388	3279	3097	4721	3939	3570	3042	2924	2784
S-7 (AS-MLV-P2)	12,103	2645	1039	$6.4 \times 10^5$	$2.2 \times 10^5$	$1.1 \times 10^6$	31,969	$1.6 \times 10^5$	$2.8 \times 10^5$

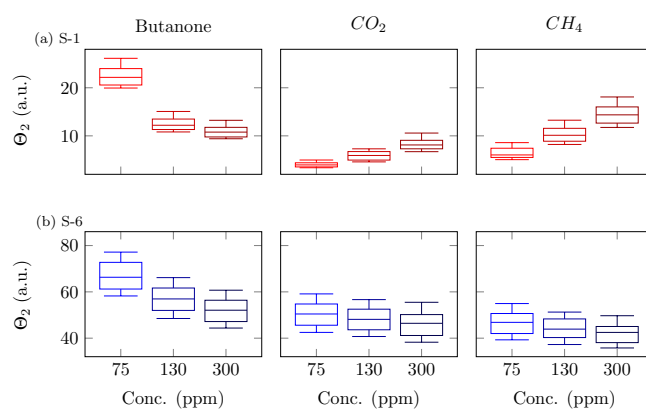


**Figure 7.** Distributions of the  $\Theta_2$  feature for the triangle pattern in the (a) S-1 (TGS2600) and (b) S-6 (TGS822) sensors. Each row represents a sensor, whereas the columns show the different compounds (i.e., butanone, carbon dioxide, and methane).

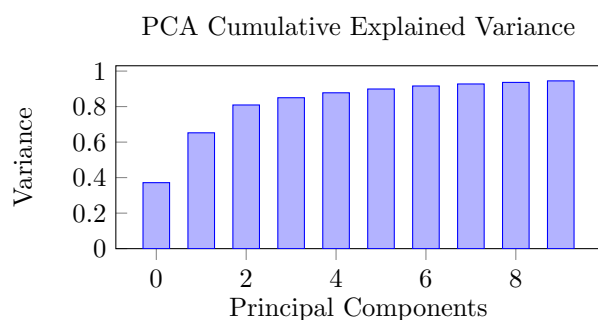


**Figure 8.** Cumulative explained variance of the first ten principal components, obtained considering all the features derived from the whole set of temperature modulations and sensors.

### 3.2. Temperature Modulation Pattern Dependency

Scatter plots of the first two principal components, obtained when applying PCA over the features extracted from all the sensors, showed different separation abilities of compounds and concentrations across the four TM patterns (Figure 9). The cumulative explained variances were 0.71, 0.73, 0.55, and 0.73 for the rectangular, sinusoidal, triangular, and rectangular–triangular (ReTr, see Figure 4d) patterns, respectively. The square wave pattern did not lead to good discrimination across compounds, especially butanone overlapped with both CO<sub>2</sub> and methane. The ability to separate concentrations was poor as well, with fewer distinct clusters. Good discrimination across compounds and concentrations was achieved using the sine wave and triangular wave patterns, even though

some uncertainty was still detected for butanone and methane. The best discrimination ability was attained when applying the combination of the square and triangular patterns (ReTr). Concentration clusters were distinct and grouped for all three compounds, being characterized by a well-defined direction for the progression of concentrations. The results of the kNN-based classification confirmed the qualitative analysis, as the ReTr TM pattern yielded a classification accuracy on the test of 100%, which is the same result obtained with the sine and triangular patterns, while the square pattern stopped at 94.4%. Even though the classification results were optimal for all patterns except the square one, the ReTr pattern was the one showing more distinct clusters for concentration values, with linear or quasi-linear relationships for changes in the concentration of the analyte (Figure 9).

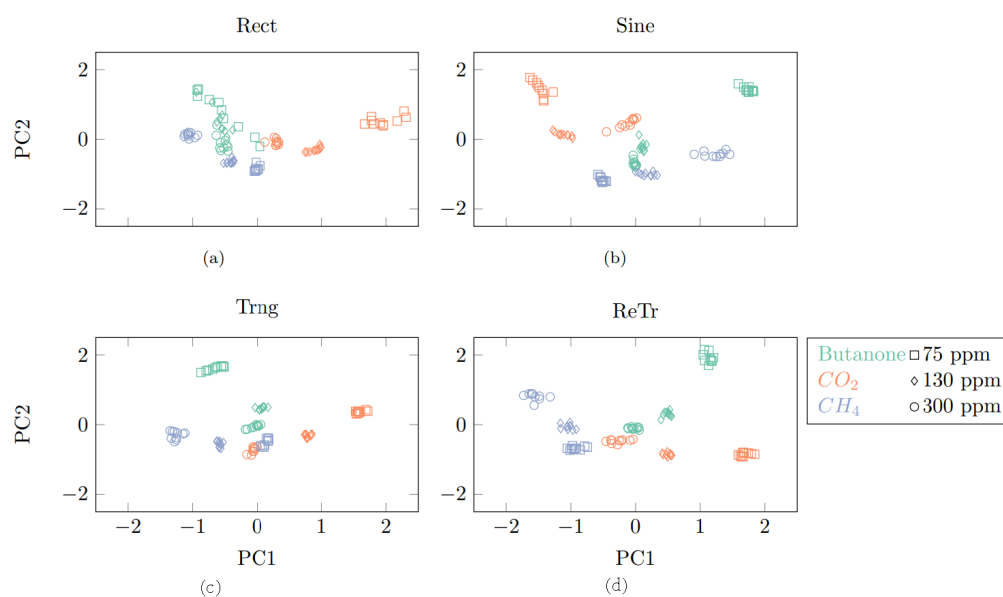


**Figure 9.** First two principal components obtained by applying PCA, considering only the features extracted from a single TM pattern, using data from all the sensors: (a) rectangular (Rect), (b) sinusoidal (Sine), (c) triangular (Trng), and (d) combination of rectangular and triangular (ReTr).

### 3.3. Sensor Type Dependency

After analyzing which TM pattern led to the optimal discrimination across compounds and concentrations, it was investigated whether one of the groups of sensors provided better results than the others. For this reason, PCA was applied separately for each group of sensors (TGS2600, TGS822, and AS-MLV-P2). The cumulative explained variances were 0.86, 0.99, and 0.99, for TGS2600, TGS822, and AS-MLV-P2 sensor types, respectively. The group of sensors providing the best discrimination based on the principal components was composed of the TGS2600 sensors (Figure 10). The TGS822 sensors showed fewer distinct clusters across compounds and concentrations, while the AS-MLV-P2 sensors were affected by a drift behavior, leading to clusters of data points less defined from a visual perspective. Even if clusters of data points were less distinct in the case of the TGS822 and AS-MLV-P2 gas sensors, kNN-based classification achieved optimal results (100%) when considering each sensor group separately, as the data points could be still discriminated in the principal components space. However, the TGS2600 sensor reported no detectable drift behavior in the principal components space, and linear or quasi-linear relationships between the principal components and the concentration of the analyte, in particular for  $\text{CH}_4$  and butanone. When considering all the features extracted from all the sensors and all the TM patterns in a bundle, the first three principal components were capable of explaining about 81% of the variance of the data (Figure 8). The first two PCA components were already capable of perfectly discriminating among concentrations and compounds (Figure 11).

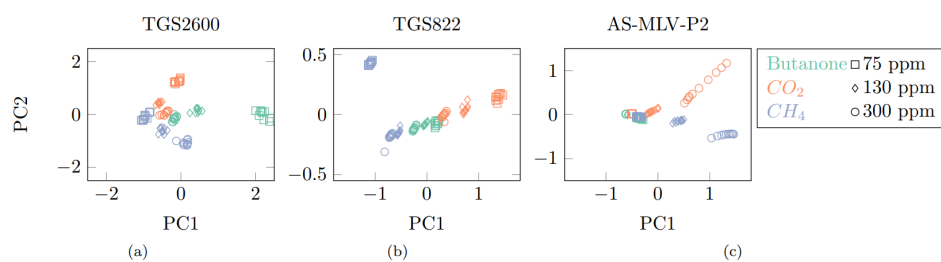


**Figure 10.** First two principal components obtained by applying PCA, considering only the features extracted from a set of sensors ((a) TGS2600, (b) TGS822, and (c) AS-MLV-P2) when the combination of rectangular and triangular waves (ReTr) was applied.

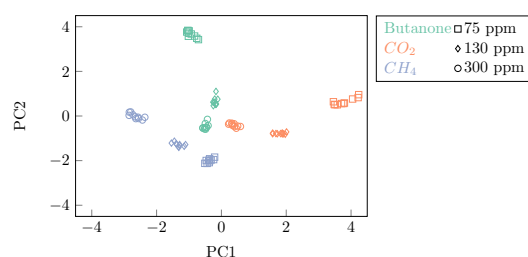


**Figure 11.** First two principal components obtained by applying PCA over the whole data set, considering all TM patterns and the whole set of sensors. Different colors refer to the different compounds that were tested. Different marker shapes refer to the different concentrations that were analyzed.

#### 4. Discussion and Conclusions

Modulating the MOS sensor temperature by applying specific voltage waveforms to the sensor heater has been documented to disclose some advantages in the measurement performance of electronic noses, such as sensitivity and selectivity enhancement, noise reduction, dynamic range expansion, and even compensation of environmental variations [41,44,51,52]. The relationship between temperature and sensor resistance has been reported to be approximately linear and inversely proportional, with the heating voltage exponentially corresponding to the sensor's temperature [42]. In this study, we addressed sensitivity and selectivity issues by testing four different TM patterns that were proposed in different earlier studies [41,53]. These patterns were applied to eight gas sensors belonging to three main classes (cfr. Table 1) embedded into a custom electronic nose, which was recently proposed by our group to examine exhaled breath in patients affected by lung cancer [13]. Three different analytes, namely methane, CO<sub>2</sub>, and butanone, featuring three varying concentrations, were tested by performing feature synthesis of the raw response data, principal component analysis, and supervised clustering. The main findings confirm that distinct TM patterns can increase the selectivity performance, even improving the ability to discriminate among different concentrations (cfr. Figure 9). Especially, by applying kNN data clustering, we found that joining sequentially square and triangular patterns provided the best results, both in selectivity and sensitivity. Remarkably, the advantage provided by the square–triangular pattern has been supported by recent findings in the literature [44]. The analysis performed on the three sensor classes led to identifying the TGS2600 type as the best sensor, providing the optimal discrimination both in the analytes and in the concentrations (cfr. Figure 10). Results from both the TGS822 and AS-MLV-P2 sensors were affected by discrimination uncertainty. Especially, AS-MLV-P2 was less effective in separating analytes and concentration, irrespective of the TM pattern. The performances of the AS-MLV-P2 could find an explanation in the conditioning period of the sensors prior to the *modulation* phase. Given the tight temporal window in which the experiments were carried out, the only way we could assess the sensors' stability was through the monitoring of their baseline resistance before the measurements. While the four TGS2600 and the two TGS822 always reached a stable baseline, drifts in the AS-MLV-P2

were observed—even if the pre-heating phase duration was comparable with the datasheet suggestion. This could explain why data referred to the S-7 and S-8 sensors were more dispersed (cfr. Figure 10c). Throughout the set of experiments, environmental data for pressure, temperature, and humidity were collected by the BME260 sensor mounted on the board. This unit monitored the environmental conditions inside the chamber. After the *wash-out* phase, the humidity settled between 10% and 13% in all trials. In their datasheets, manufacturers provide sensor resistance variations based on temperature/humidity dependencies, with relative humidity spanning from 30–35% to 80–95–100%, hence out of our working range. For this reason, despite the fact that humidity plays an important role in modifying the sensor behavior, at this stage humidity analysis was not performed. Additional data will be collected in future experiments to investigate the influence of humidity and to develop compensation algorithms that can at least mitigate its impact. The results obtained in the present study are in line with the earlier literature. More than a decade ago, simulations using electronic CAD software demonstrated the benefits of temperature modulation in MOS sensors. Experiments based on such simulations confirmed that a single sensor (TGS2600, Figaro Inc., Mino, Japan) device could achieve both optimal gas identification and accurate concentration (range: 10–50 ppm) determination simultaneously [42]. Specific TM patterns induced by a heating voltage spike, prior to a voltage step, were proposed to detect 12 different airborne analytes using a single sensor (SP3-AQ2, FIS Inc., Edmonds, WA, USA) [41]. While the identification of such contaminants was reported to be effective, the tested concentrations ranged from 300 to 2500 ppm, sensibly higher than traditional VOCs concentrations in exhaled breath. Gas identification accuracy was reported to improve when properly modulating sensor temperature, applying wavelet transform to sensor responses to extract representative features, and classification based on machine learning [52]. In such a study, methanol, ethanol, and butanone analytes were tested by scanning concentrations from 100–2000 ppm, obtaining a compound discrimination accuracy of about 92%. More recently, various experiments performed with commercial MOS gas sensors reported the feasibility of simultaneous gas classification and gas concentration prediction using TGS2620 and TGS2602 sensor types (Figaro Inc.) and advanced data analysis based on support vector machines [53]. Results on three different gases, namely CO, NO<sub>2</sub>, and HCHO, showed compound discrimination accuracy close to 100% when applying the stair TM pattern.

In terms of clinical feasibility, it is important to note that exhaled breath constitutes a highly intricate mixture. This complexity can pose various challenges during analysis. As a matter of fact, to date, no compound or group of compounds has been found with the capability to indicate the presence of disease through exhaled breath [2]. In addition, many confounding factors such as a subject's diet, smoking habits, and breath sample collection pose challenges that need to be tackled when establishing a standardized clinical testing protocol. In our previous work [13], we presented the outcomes of a preclinical study involving the analysis of exhaled breath from a population of patients with lung cancer. This was compared against a control group. An earlier version of the apparatus outlined in this paper was employed. Although the results were consistent with similar studies reported in the literature, the protocol had been customized to accommodate specific conditions related to breath sample collection, limiting the potential for large-scale comparisons. Consequently, the acquisition of data from a substantial cohort of subjects is crucial for the development of accurate machine learning algorithms that consider these variables in their decision-making. The standardization of protocols for breath collection and the analysis of exhaled breath data from a sizable and diverse subject pool could effectively mitigate the influence of these factors.

Some limitations of the present study need to be highlighted. First of all, in this work, the same TM pattern was applied at the same time to the whole set of gas sensors. In the future, it could be interesting to apply different patterns to different groups of sensors, to see whether discrimination capabilities and sensitivity could be improved even more. This working hypothesis comes from the fact that, as demonstrated in this work, there

is a performance dependency of different sensors on the different modulation patterns. In addition, it would be interesting to test the device in a more complex environment, in which the air sample is composed of a mixture of compounds, to determine whether the system is capable of simultaneously distinguishing specific analytes, and at which level. In this manner, conducting a comprehensive investigation into the correlation between temperature modulation and compound identification across various sensor types within a complex environment will enable us to apply a wide range of modulation techniques throughout the sensor array. This approach will effectively mitigate the cross-sensitivity and selectivity challenges faced by individual sensors, enhancing their discrimination performances. One last point can be made on the absence of oxygen in the carrier gas. Oxygen molecules can adsorb on the sensor's surface, generating active sites that will act as a potential barrier and prevent electron conduction. This way, the background conductance of the sensor itself decreases. In the presence of reducing species, the adsorbed oxygen will detach from the surface to bind with the gaseous analyte, leading to an increase in conductance. As a result, the resolution of the sensor increases. In addition, the higher the oxygen content is, the higher the formation rate of active sites is, and hence the recovery time of the sensor can be improved. Despite the clear advantages of having fractions of oxygen in the carrier gas, one work conducted specifically on the TGS822 [54] observed no drastic changes in the actual sensitivity of the sensor, even when varying the oxygen content in the carrier gas. According to the aim of our work, the testing protocol was conceived to study the detection sensitivity as a function of sensor temperature driving alone. The analyzed gases were not diluted in clean air but only mixed with nitrogen, which actually represents the worst-case scenario in terms of sensor performance. In view of the highlighted mechanisms, if our work showed good discrimination capabilities in the absence of oxygen, the authors believe that its introduction could even enhance the performance of the device. In addition, one can expect that the effect of oxygen has a quantifiable impact on the sensor response, and this impact could be put in relation to the oxygen content and calibrated [55]. Nonetheless, even if this study had a specific span of research, it demonstrated the scalability of the proposed electronic nose with an integrated TM control and the feasibility of fruitfully applying TM patterns to improve the detection ability of VOCs. This study was in fact designed with a small number of target analytes as a starting point. Technically, once a new analyte needs to be detected, one could explore—offline—the best combination of sensor and temperature modulation pattern for its discrimination and then implement it in the electronic nose. This will allow for further exploration of the detection quality of the system for additional target analytes, which feature clinical value and are present in the exhaled breath. In conclusion, we remark that this work may bring the use of TM-based electronic noses incrementally closer to clinical translation.

**Author Contributions:** Conceptualization, P.C.; methodology, P.C.; software, A.R. and D.M.; experimental measurements, A.R. and S.G.; formal analysis, A.R. and D.M.; investigation, P.C.; resources, P.C.; data curation, A.R. and D.M.; writing—original draft preparation, A.R., D.M., F.C. and P.C.; writing—review and editing, A.R., D.M., F.C. and P.C.; visualization, A.R. and D.M.; supervision, P.C.; project administration, F.C. and P.C.; funding acquisition, F.C. and P.C. All authors have read and agreed to the published version of the manuscript.

**Funding:** The work of A.R. is partially funded by the Ph.D. Interdisciplinary program, Doctoral School of the Politecnico di Milano, and funded by PNRR-PE, Future Artificial Intelligence Research (FAIR)—Italian Ministry of University and Research.

**Institutional Review Board Statement:** Not applicable.

**Informed Consent Statement:** Not applicable.

**Data Availability Statement:** Not applicable.

**Acknowledgments:** The authors would like to express their gratitude to Damiano Rosario Tasso for his valuable contribution in the development of the electronic nose prototype.

**Conflicts of Interest:** The authors declare no conflict of interest.

### Abbreviations

The following abbreviations are used in this manuscript:

CV	Cross-validation
COPD	Chronic obstructive pulmonary disease
GC–MS	Gas chromatography–mass spectrometry
MOS	Metal oxide semiconductor
kNN	k-nearest neighbors
LDCT	Low-dose computed tomography
PCA	Principal component analysis
PCB	Printed circuit board
ppb	Parts per billion
ppm	Parts per million
SVM	Support vector machine
VOCs	Volatile organic compounds
MCU	Microcontroller unit
PTFE	Polytetrafluoroethylene
TM	Temperature modulation
VOC	Volatile organic compound

### References

- Amann, A.; Miekisch, W.; Schubert, J.; Buszewski, B.; Ligor, T.; Jezierski, T.; Pleil, J.; Risby, T. Analysis of exhaled breath for disease detection. *Annu. Rev. Anal. Chem.* **2014**, *7*, 455–482. [[CrossRef](#)] [[PubMed](#)]
- Marzorati, D.; Mainardi, L.; Sedda, G.; Gasparri, R.; Spaggiari, L.; Cerveri, P. A Review of Exhaled Breath: A Key Role in Lung Cancer Diagnosis. *J. Breath Res.* **2019**, *13*, 034001. [[CrossRef](#)] [[PubMed](#)]
- Davis, M.D.; Fowler, S.J.; Montpetit, A.J. Exhaled breath testing—A tool for the clinician and researcher. *Paediatr. Respir. Rev.* **2019**, *29*, 37–41. [[CrossRef](#)] [[PubMed](#)]
- Dragonieri, S.; Schot, R.; Mertens, B.J.A.; Le Cessie, S.; Gauw, S.A.; Spanevello, A.; Resta, O.; Willard, N.P.; Vink, T.J.; Rabe, K.F.; et al. An electronic nose in the discrimination of patients with asthma and controls. *J. Allergy Clin. Immunol.* **2007**, *120*, 856–862. [[CrossRef](#)] [[PubMed](#)]
- Dragonieri, S.; Annema, J.T.; Schot, R.S.; van der Schee, M.P.C.; Spanevello, A.; Carratú, P.; Resta, O.; Rabe, K.F.; Sterk, P.J. An electronic nose in the discrimination of patients with non-small cell lung cancer and COPD. *Lung Cancer* **2009**, *64*, 166–170. [[CrossRef](#)]
- Peng, G.; Hakim, M.; Broza, Y.Y.; Billan, S.; Abdah-Bortnyak, R.; Kuten, A.; Tisch, U.; Haick, H. Detection of lung, breast, colorectal, and prostate cancers from exhaled breath using a single array of nanosensors. *Br. J. Cancer* **2010**, *103*, 542–551. [[CrossRef](#)]
- Hanna, G.B.; Boshier, P.R.; Markar, S.R.; Romano, A. Accuracy and Methodologic Challenges of Volatile Organic Compound–Based Exhaled Breath Tests for Cancer Diagnosis. *JAMA Oncol.* **2019**, *5*, e182815. [[CrossRef](#)]
- Ratiu, I.A.; Ligor, T.; Bocos-Bintintan, V.; Mayhew, C.A.; Buszewski, B. Volatile Organic Compounds in Exhaled Breath as Fingerprints of Lung Cancer, Asthma and COPD. *J. Clin. Med.* **2021**, *10*, 32. [[CrossRef](#)]
- Taverna, G.; Grizzi, F.; Tidu, L.; Bax, C.; Zanoni, M.; Vota, P.; Lotesoriere, B.J.; Prudenza, S.; Magagnin, L.; Langfelder, G.; et al. Accuracy of a new electronic nose for prostate cancer diagnosis in urine samples. *Int. J. Urol.* **2022**, *29*, 890–896. [[CrossRef](#)]
- Montuschi, P. Analysis of exhaled breath condensate in respiratory medicine: Methodological aspects and potential clinical applications. *Ther. Adv. Respir. Dis.* **2007**, *1*, 5–23. [[CrossRef](#)]
- Hakim, M.; Broza, Y.Y.; Barash, O.; Peled, N.; Phillips, M.; Amann, A.; Haick, H. Volatile Organic Compounds of Lung Cancer and Possible Biochemical Pathways. *Chem. Rev.* **2012**, *112*, 5949–5966. [[CrossRef](#)]
- Beccaria, M.; Mellors, T.R.; Petion, J.S.; Rees, C.A.; Nasir, M.; Systrom, H.K.; Sairistil, J.W.; Jean-Juste, M.A.; Rivera, V.; Lavoile, K.; et al. Preliminary investigation of human exhaled breath for tuberculosis diagnosis by multidimensional gas chromatography—Time of flight mass spectrometry and machine learning. *J. Chromatogr. B Anal. Technol. Biomed. Life Sci.* **2018**, *1074–1075*, 46–50. [[CrossRef](#)] [[PubMed](#)]
- Marzorati, D.; Mainardi, L.; Sedda, G.; Gasparri, R.; Spaggiari, L.; Cerveri, P. MOS Sensors Array for the Discrimination of Lung Cancer and At-Risk Subjects with Exhaled Breath Analysis. *Chemosensors* **2021**, *9*, 209. [[CrossRef](#)]
- Amor, R.E.; Nakhleh, M.K.; Barash, O.; Haick, H. Breath analysis of cancer in the present and the future. *Eur. Respir. Rev.* **2019**, *28*, 190002. [[CrossRef](#)] [[PubMed](#)]
- Rudnicka, J.; Kowalkowski, T.; Ligor, T.; Buszewski, B. Determination of volatile organic compounds as biomarkers of lung cancer by SPME-GC-TOF/MS and chemometrics. *J. Chromatogr. B Anal. Technol. Biomed. Life Sci.* **2011**, *879*, 3360–3366. [[CrossRef](#)]

16. Buszewski, B.; Ligor, T.; Jezierski, T.; Wenda-Piesik, A.; Walczak, M.; Rudnicka, J. Identification of volatile lung cancer markers by gas chromatography-mass spectrometry: Comparison with discrimination by canines. *Anal. Bioanal. Chem.* **2012**, *404*, 141–146. [[CrossRef](#)]
17. Phillips, M.; Cataneo, R.N.; Cummin, A.R.C.; Gagliardi, A.J.; Gleeson, K.; Greenberg, J.; Maxfield, R.A.; Rom, W.N. Detection of Lung Cancer With Volatile Markers in the Breath. *Chest* **2003**, *123*, 2115–2123. [[CrossRef](#)]
18. Machado, R.F.; Laskowski, D.; Deffenderfer, O.; Burch, T.; Zheng, S.; Mazzone, P.J.; Mekhail, T.; Jennings, C.; Stoller, J.K.; Pyle, J.; et al. Detection of Lung Cancer by Sensor Array Analyses of Exhaled Breath. *Am. J. Respir. Crit. Care Med.* **2005**, *171*, 1286–1291. [[CrossRef](#)]
19. Bajtarevic, A.; Ager, C.; Pienz, M.; Klieber, M.; Schwarz, K.; Ligor, M.; Ligor, T.; Filipiak, W.; Denz, H.; Fiegl, M.; et al. Noninvasive detection of lung cancer by analysis of exhaled breath. *BMC Cancer* **2009**, *9*, 348. [[CrossRef](#)]
20. Ligor, T.; Pater, Ł.; Buszewski, B. Application of an artificial neural network model for selection of potential lung cancer biomarkers. *J. Breath Res.* **2015**, *9*, 027106. [[CrossRef](#)]
21. Schallschmidt, K.; Becker, R.; Jung, C.; Bremser, W.; Walles, T.; Neudecker, J.; Leschber, G.; Frese, S.; Nehls, I. Comparison of volatile organic compounds from lung cancer patients and healthy controls—challenges and limitations of an observational study. *J. Breath Res.* **2016**, *10*, 046007. [[CrossRef](#)] [[PubMed](#)]
22. Kononov, A.; Korotetsky, B.; Jahatspanian, I.; Gubal, A.; Vasiliev, A.; Arsenjev, A.; Nefedov, A.; Barchuk, A.; Gorbunov, I.; Kozyrev, K.; et al. Online breath analysis using metal oxide semiconductor sensors (electronic nose) for diagnosis of lung cancer. *J. Breath Res.* **2019**, *14*, 016004. [[CrossRef](#)] [[PubMed](#)]
23. Liu, L.; Li, W.; He, Z.; Chen, W.; Liu, H.; Chen, K.; Pi, X. Detection of lung cancer with electronic nose using a novel ensemble learning framework. *J. Breath Res.* **2021**, *15*, 026014. [[CrossRef](#)] [[PubMed](#)]
24. Dragonieri, S.; Pennazza, G.; Carratu, P.; Resta, O. Electronic Nose Technology in Respiratory Diseases. *Lung* **2017**, *195*, 157–165. [[CrossRef](#)]
25. van de Goor, R.; van Hooren, M.; Dingemans, A.M.; Kremer, B.; Kross, K. Training and Validating a Portable Electronic Nose for Lung Cancer Screening. *J. Thorac. Oncol.* **2018**, *13*, 676–681. [[CrossRef](#)]
26. Di Natale, C.; Macagnano, A.; Martinelli, E.; Paolesse, R.; D’Arcangelo, G.; Roscioni, C.; Finazzi-Agrò, A.; D’Amico, A. Lung cancer identification by the analysis of breath by means of an array of non-selective gas sensors. *Biosens. Bioelectron.* **2003**, *18*, 1209–1218. [[CrossRef](#)]
27. D’Amico, A.; Pennazza, G.; Santonico, M.; Martinelli, E.; Roscioni, C.; Galluccio, G.; Paolesse, R.; Di Natale, C. An investigation on electronic nose diagnosis of lung cancer. *Lung Cancer* **2010**, *68*, 170–176. [[CrossRef](#)]
28. Peng, G.; Tisch, U.; Adams, O.; Hakim, M.; Shehada, N.; Broza, Y.Y.; Billan, S.; Abdah-Bortnyak, R.; Kuten, A.; Haick, H. Diagnosing lung cancer in exhaled breath using gold nanoparticles. *Nat. Nanotechnol.* **2009**, *4*, 669–673. [[CrossRef](#)]
29. Mazzone, P.J.; Wang, X.F.; Xu, Y.; Mekhail, T.; Beukemann, M.C.; Na, J.; Kemling, J.W.; Suslick, K.S.; Sasidhar, M. Exhaled Breath Analysis with a Colorimetric Sensor Array for the Identification and Characterization of Lung Cancer. *J. Thorac. Oncol.* **2012**, *7*, 137–142. [[CrossRef](#)]
30. Zhong, X.; Li, D.; Du, W.; Yan, M.; Wang, Y.; Huo, D.; Hou, C. Rapid recognition of volatile organic compounds with colorimetric sensor arrays for lung cancer screening. *Anal. Bioanal. Chem.* **2018**, *410*, 3671–3681. [[CrossRef](#)]
31. Saruhan, B.; Fomekong, R.L.; Nahirniak, S. Review: Influences of Semiconductor Metal Oxide Properties on Gas Sensing Characteristics. *Front. Sens.* **2021**, *2*, 657931. [[CrossRef](#)]
32. Wilson, A.D.; Baietto, M. Applications and advances in electronic-nose technologies. *Sensors* **2009**, *9*, 5099–5148. [[CrossRef](#)] [[PubMed](#)]
33. Blatt, R.; Bonarini, A.; Calabro, E.; Torre, M.D.; Matteucci, M.; Pastorino, U. Lung Cancer Identification by an Electronic Nose based on an Array of MOS Sensors. In Proceedings of the 2007 International Joint Conference on Neural Networks, Orlando, FL, USA, 12–17 August 2007. [[CrossRef](#)]
34. Kou, L.; Zhang, D.; Liu, D. A Novel Medical E-Nose Signal Analysis System. *Sensors* **2017**, *17*, 402. [[CrossRef](#)] [[PubMed](#)]
35. Santos, V.; Freitas, C.; Fernandes, M.G.; Sousa, C.; Reboledo, C.; Cruz-Martins, N.; Mosquera, J.; Hespanhol, V.; Campelo, R. Liquid biopsy: The value of different bodily fluids. *Biomark. Med.* **2022**, *16*, 127–145. [[CrossRef](#)] [[PubMed](#)]
36. Ulanowska, A.; Kowalkowski, T.; Trawińska, E.; Buszewski, B. The application of statistical methods using VOCs to identify patients with lung cancer. *J. Breath Res.* **2011**, *5*, 046008. [[CrossRef](#)]
37. Rudnicka, J.; Kowalkowski, T.; Buszewski, B. Searching for selected VOCs in human breath samples as potential markers of lung cancer. *Lung Cancer* **2019**, *135*, 123–129. [[CrossRef](#)]
38. Sears, W.; Colbow, K.; Consadori, F. Algorithms to improve the selectivity of thermally-cycled tin oxide gas sensors. *Sens. Actuators* **1989**, *19*, 333–349. [[CrossRef](#)]
39. Cavicchi, R.; Suehle, J.; Kreider, K.; Gaitan, M.; Chaparala, P. Fast temperature programmed sensing for micro-hotplate gas sensors. *IEEE Electron. Device Lett.* **1995**, *16*, 286–288. [[CrossRef](#)]
40. Cavicchi, R.; Suehle, J.; Kreider, K.; Gaitan, M.; Chaparala, P. Optimized temperature-pulse sequences for the enhancement of chemically specific response patterns from micro-hotplate gas sensors. *Sens. Actuators B Chem.* **1996**, *33*, 142–146. [[CrossRef](#)]
41. Hossein-Babaei, F.; Amini, A. A breakthrough in gas diagnosis with a temperature-modulated generic metal oxide gas sensor. *Sens. Actuators B Chem.* **2012**, *166–167*, 419–425. [[CrossRef](#)]

42. Martinelli, E.; Polese, D.; Catini, A.; D'Amico, A.; Di Natale, C. Self-adapted temperature modulation in metal-oxide semiconductor gas sensors. *Sens. Actuators B Chem.* **2012**, *161*, 534–541. [[CrossRef](#)]
43. Gosangi, R.; Gutierrez-Osuna, R. Active Temperature Programming for Metal-Oxide Chemoresistors. *IEEE Sens. J.* **2010**, *10*, 1075–1082. [[CrossRef](#)]
44. Wu, Z.; Zhang, H.; Ji, H.; Yuan, Z.; Meng, F. Novel combined waveform temperature modulation method of NiO-In<sub>2</sub>O<sub>3</sub> based gas sensor for measuring and identifying VOC gases. *J. Alloys Compd.* **2022**, *918*, 165510. [[CrossRef](#)]
45. Li, W.; Liu, H.; Xie, D.; He, Z.; Pi, X. Lung Cancer Screening Based on Type-different Sensor Arrays. *Sci. Rep.* **2017**, *7*, 1969. [[CrossRef](#)] [[PubMed](#)]
46. Infineon Technologies. *PSoC 5LP: CY8C58LP Family Datasheet*; Cypress Semiconductor Corporation: San Jose, CA, USA, 2019.
47. Robert Bosch GmbH. *BME280 Datasheet*; Bosch Sensortec: Kusterdingen, Germany, 2018.
48. de Lacy Costello, B.P.J.; Ledochowski, M.; Ratcliffe, N.M. The importance of methane breath testing: A review. *J. Breath Res.* **2013**, *7*, 024001. [[CrossRef](#)]
49. Szabó, A.; Ruzsanyi, V.; Unterkofler, K.; Mohácsi, A.; Tuboly, E.; Boros, M.; Szabó, G.; Hinterhuber, H.; Amann, A. Exhaled methane concentration profiles during exercise on an ergometer. *J. Breath Res.* **2015**, *9*, 016009. [[CrossRef](#)]
50. Fu, X.A.; Li, M.; Knipp, R.J.; Nantz, M.H.; Bousamra, M. Noninvasive detection of lung cancer using exhaled breath. *Cancer Med.* **2014**, *3*, 174–181. [[CrossRef](#)]
51. Wang, C.; Yin, L.; Zhang, L.; Xiang, D.; Gao, R. Metal oxide gas sensors: Sensitivity and influencing factors. *Sensors* **2010**, *10*, 2088–2106. [[CrossRef](#)]
52. Amini, A.; Bagheri, M.A.; Montazer, G.A. Improving gas identification accuracy of a temperature-modulated gas sensor using an ensemble of classifiers. *Sens. Actuators B Chem.* **2013**, *187*, 241–246. [[CrossRef](#)]
53. Yin, X.; Zhang, L.; Tian, F.; Zhang, D. Temperature Modulated Gas Sensing E-Nose System for Low-Cost and Fast Detection. *IEEE Sens. J.* **2016**, *16*, 464–474. [[CrossRef](#)]
54. Sriyudthsak, M.; Promsong, L.; Panyakeow, S. Effect of carrier gas on response of oxide semiconductor gas sensor. *Sens. Actuators B Chem.* **1993**, *13*, 139–142. [[CrossRef](#)]
55. Shah, A.; Laurent, O.; Lienhardt, L.; Broquet, G.; Rivera Martinez, R.; Allegrini, E.; Ciaï, P. Characterising the methane gas and environmental response of the Figaro Taguchi Gas Sensor (TGS) 2611-E00. *Atmos. Meas. Tech.* **2023**, *16*, 3391–3419. [[CrossRef](#)]

**Disclaimer/Publisher's Note:** The statements, opinions and data contained in all publications are solely those of the individual author(s) and contributor(s) and not of MDPI and/or the editor(s). MDPI and/or the editor(s) disclaim responsibility for any injury to people or property resulting from any ideas, methods, instructions or products referred to in the content.